Available online at www.sciencedirect.com
SCIENCE DIRECT®
Journal of Hydrology 284 (2003) 131–150
Journal of Hydrology
www.elsevier.com/locate/jhydrol

Green element simulations of multiaquifer flows with a time-dependent Green's function

Akpofure E. Taigbenu*

Department of Civil and Water Engineering, National University of Science and Technology, Box AC939, Bulawayo, Zimbabwe

Received 2 September 2002; accepted 25 July 2003

Abstract

A new formulation of the Green element method (GEM), based on the transient Green's function of the diffusion differential operator, is herein used to solve the problem of transient flow in multiply layered aquifers that are separated by aquitards (leaky strata) which provide hydraulic interactions between them. By adopting the commonly used hydraulic flow approximation, flow in the aquifers is considered to take place in two lateral dimensions and in one vertical direction in the aquitards. As with an earlier GE multiaquifer model, the current model solves the one-dimensional flow in the aquitards by the formulation of [Appl. Math. Model. 22 (1998) 687] but uses the transient Green's function of the diffusion operator to solve the two-dimensional aquifer flow instead of the logarithmic Green's function formulation of [Water Resour. Res. 36 (2000) 3631]. In essence, the current formulation uses the same form of Green's functions for both flows in the aquifers and aquitards. While this can be viewed as an advantage of the current formulation over the previous one, the former presents other computational challenges and intricacies that are discussed in this paper. Applying the current formulation, and incorporating a Picard-type iterative algorithm, solutions are provided for regional flows in heterogeneous multiaquifer systems of arbitrary geometries that are subjected to point and distributed recharge of arbitrary strengths.

Keywords: Groundwater flow; Multiaquifer; Green's function; Numerical solutions

1. Introduction

Groundwater systems are known to exist as multilayered aquifers that are separated by leaky strata through which the transport of water occurs by an amount dependent on their areal extent, fluid transmitting and storage capacities and the hydraulic gradients at the aquifer–aquitard interfaces. Since the pioneering work of Theis (1935), hydrologists have shown considerable interest in studying the mechanisms of flow and storage of water in these systems.

In modelling multiaquifer systems, two approaches have generally been followed. These are the hydrodynamic one which correctly treats the flow as three dimensional and a hydraulic one which approximates flow variables as depth-averaged quantities in the aquifers so that flow is essentially horizontal while that in the aquitards is

* Tel.: +263-9-282007; fax: +263-9-286803.
E-mail address: taigbenu@hotmail.com (A.E. Taigbenu).

0022-1694/$ - see front matter © 2003 Elsevier B.V. All rights reserved.
doi:10.1016/j.jhydrol.2003.07.002

one dimensional in the vertical direction. The latter approach is now widely accepted in hydrogeological circles by virtue of the fact that the enormity of the computing resources required in solving large regional multiaquifer systems with the hydrodynamic model cannot be justified, and also because hydrogeological parameters that are obtained from field pumping tests reflect depth-averaged 2-D flow properties. In practice, the hydraulic approach is justified as long as the contrast in hydraulic conductivity values between the aquifers and aquitards are of two orders of magnitude.

Following the hydraulic approach, solution strategies have, broadly speaking, proceeded along a number of directions. Analytical strategies can be traced to the work of Theis who, using similar concepts of heat transfer in an infinite domain, provided the solution to confined flow to a constant discharging well in an infinitely extensive homogeneous aquifer (Theis, 1935). To accommodate the complexities of multiply layered aquifers, the solution of Theis was later extended by Jacob and Hantush to include an overlying aquitard and unconfined aquifer (Jacob, 1946; Hantush and Jacob, 1955). However, in their solutions, they failed to fully take into consideration the elastic storage property of the leaky stratum, while assuming the water table level in the unconfined medium remained the same for all times as the underlying aquifer was being pumped. The analytical solution of Neuman and Witherspoon (1969a,b) for two laterally infinitely extensive confined aquifers separated by an aquitard fully accounted for these elastic storage effects, and their works are therefore considered as the pioneering analytical solutions for truly multiaquifer systems. Though these analytic solutions are quite useful in the estimation of hydrogeological parameters from field investigations, they are however of limited use in modelling aquifer systems of arbitrary geometries with point and distributed recharge of arbitrary strengths in space and time.

Computational techniques have largely overcome many of the limitations of analytical solution strategies. To that end, finite difference (FD), finite element (FE), analytic element (AE), boundary element (BE) and lately Green element (GE) methods have been applied. They have either been applied to the coupled aquifer–aquitard equations along the lines of the theory of Neuman and Witherspoon (1969a) or to the integro-differential equations of Herrera (1970). Making use of the former theory are the FE model of Chorley and Frind (1978), the BE model of Zakikhani and Aral (1989) and the GE model of Taigbenu and Onyejekwe (2000), while the latter theory has been incorporated into the FE model of Herrera and Yates (1977), the FD models of Premchitt (1981); Cheng and Ou (1989), and the BE models of Cheng and Morohunfola (1993). The AE method has been largely limited in application to steady groundwater flows (Strack, 1999).

In the current work, the Green element method (GEM) is applied to the multiaquifer flow problem along the lines of the theory of Neuman and Witherspoon (1969a) using the transient Green's function of the diffusion differential operator in contrast to the logarithmic Green's function earlier employed in the model of Taigbenu and Onyejekwe (2000). As a brief review of the GEM, its theory is founded on the singular boundary integral theory that is also utilized in the boundary element method (BEM), while its computational implementation involves evaluating the integral equation from element to element and imposing the compatibility requirements at inter-element boundaries, so that a banded global coefficient matrix is achieved (Taigbenu, 1999). The element-by-element approach adopted in GEM lends its solution process to local nodal support in contrast to BEM which lends itself to global nodal support so that GEM is more amenable to handling nonlinearities and medium heterogeneities. The method is applied to both the 1-D flow in aquitards and the 2-D flow in the aquifers. We have earlier demonstrated in Taigbenu and Onyejekwe (2000) the superiority of the GEM over the FEM of Chorley and Frind (1978) in calculating the leakage flux through the aquitards, and that is not repeated here. The superiority of that GEM solution is primarily because of its numerical feature of direct computation of the leakage flux in contrast to most other methods that calculate the flux by numerical differentiation of the hydraulic heads. This paper compares the solutions of multiply-layered aquifers obtained from two GE models, one based on the transient Green's function of the diffusion operator,

herein referred to as model 2, and an earlier one based on the logarithmic Green's function, referred to as model 1. The model herein developed has the capability of simulating flows in multiaquifer systems with alternating layers of heterogeneous aquifers and aquitards of varying thicknesses that are variously stressed point-wise and in a distributed fashion. Three examples are used to demonstrate the performance of both models. The results indicate that the GE models are quite suited to groundwater well hydraulics in the sense that grid refinement in the vicinity of wells, as commonly done in other numerical methods, is avoided. This is because of the singular nature of the Green's functions which allows the singular contribution from the wells to be correctly represented. The first two examples have exact solutions with which the accuracy of the current model is assessed. The third example of four aquifers and three aquitards with various abstraction stresses serve to demonstrate the capabilities of the current model in handling practically realistic multiaquifer flows. Two flow scenarios of that example are examined: one with the uppermost aquifer being confined and the other being unconfined and recharged naturally. In addition, there is excellent agreement between the solutions of the current model (model 2) and those of the previous one (model 1), although the latter uses less CPU time per simulation than the current model.

2. Flow equations

In examining the flow in a multiaquifer system, consideration is given to a generalized system of M aquifers that are separated by $M-1$ aquitards. Though not always the case, the uppermost aquifer is taken to be an unconfined one. In line with the approximate hydraulic flow theory of Neuman and Witherspoon (1969a), the flow in each of the aquifers is treated as essentially horizontal so that flow variables do not vary with depth or alternatively considered as depth-averaged quantities. Aquifer properties are assumed to remain the same in all directions (isotropy) but can vary from one location to another (heterogeneity). Furthermore, the thickness of aquifers is allowed to have spatial variation. The flow through the aquitards is one-dimensional in the vertical direction, and it represents the leakage flux in and out of the aquifers. For the ith confined aquifer, the governing equation is (Bear, 1979)

$$\nabla(T\nabla h)_i + q_L|_{z_i^t} - q_L|_{z_i^b} = \left(n\frac{\partial h}{\partial t}\right)_i + f_i(x,y,t) + p_i \qquad (1)$$

while that for the Mth unconfined aquifer is

$$\nabla(T\nabla h)_M - q_L|_{z_M^b} = \left(n\frac{\partial h}{\partial t}\right)_M + f_M(x,y,t) + p_M \qquad (2)$$

It should be noted that Eq. (2) takes the form of Eq. (1) if the uppermost aquifer is confined. The variables in Eqs. (1) and (2) have the following definitions: $h \equiv h(x,y,t)$ is the piezometric head (confined) or water table elevation (unconfined), $\nabla = i\partial/\partial x + j\partial/\partial y$ is the two-dimensional gradient operator, $T = Kb$ denotes the transmissivity, where K is the hydraulic conductivity, b is the saturated flow thickness, $n = Cb$, for the confined case, is the storativity or coefficient of storage, where C is the specific storage, and for the unconfined case n is the specific yield of the aquifer. The leakage flux through the aquitards into the aquifers is denoted as q_L, while z_i^t and z_i^b are the z-coordinates of the top and bottom of the ith aquifer that has a thickness of $b_i = z_i^t - z_i^b$ (see Fig. 1). The contribution due to distributed recharge sources is denoted as f, while that due to point sources and sinks is p. The contribution from point sources is expressed mathematically as

$$p = \sum_{w=1}^{N_w} Q_w(t)\delta(x - x_w)\delta(y - y_w) \qquad (3)$$

where $Q_w(t)$ is the strength or discharge rate of a well located at (x_w, y_w), δ is the Dirac delta function, and N_w is the number of such wells. It is assumed all the aquifers have the same areal extent, and appropriate boundary conditions can be prescribed on the boundary of each of the aquifers. Those boundary conditions are either a known distribution of hydraulic head, say, a known water elevation at the boundary where a large water body adjoins the aquifer. In that case, the condition on the ith aquifer

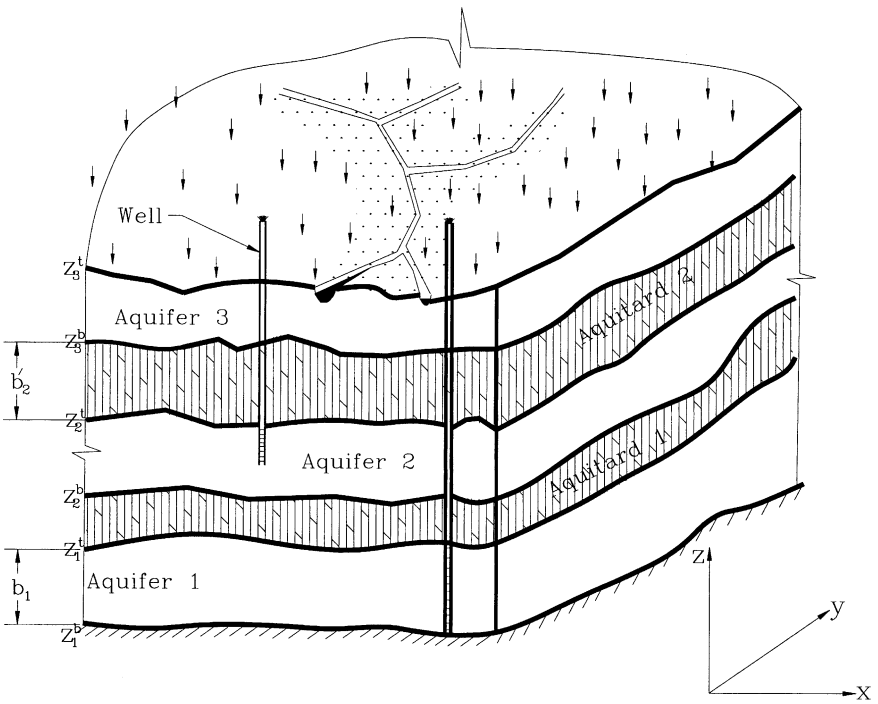

Fig. 1. Representation and definitive sketch of a multiaquifer system.

is described as

$$h_i(x,y,t) = H_i(x,y,t) \text{ on } \Gamma_i^1 \tag{4a}$$

In a case where the flux in or out of the aquifer is known, the condition is given by

$$\left(-T\frac{\partial h}{\partial n}\right)_i = q_i(x,y,t) \text{ on } \Gamma_i^2 \tag{4b}$$

in which q is the normal flux and $\Gamma = \Gamma^1 + \Gamma^2$ is the boundary of the aquifer. A linear combination of the above two conditions can be accommodated where there exists, say, a ponded recharge surface over a thin leaky stratum on the uppermost aquifer. Since we are dealing with a time-dependent problem, the distribution of hydraulic head in all aquifers is assumed known at some initial time t_0.

The leakage fluxes into the aquifers, denoted by q_L in Eqs. (1) and (2), are obtained from solving the transient one-dimensional flow equation that, for the ith leaky stratum, is given by

$$\left[\frac{\partial}{\partial z}\left(K'\frac{\partial h'}{\partial z}\right)\right]_i = \left(C'\frac{\partial h'}{\partial t}\right)_i \tag{5}$$

in which K' is the hydraulic conductivity, h' is the hydraulic head in the aquitard, and C' is the specific storage. Dirichlet boundary conditions are specified on the upper and lower surfaces of the aquitards. These are values of hydraulic heads in the aquifers that are above and below the ith aquitard, and they are represented as

$$h_i'(z_{i+1}^b, t) = h_{i+1}(t) \tag{6a}$$

$$h_i'(z_i^t, t) = h_i(t) \tag{6b}$$

It is also expected that the hydraulic heads in the aquitards are known at the initial time. The flow in the M aquifers and $M-1$ aquitards is obtained by coupling Eqs. (1) and (2) with Eq. (5) through the leakage flux that takes place at the aquifer–aquitard interfaces. This flux at the interface of the top of the ith

aquifer and the bottom of the ith aquitard (Fig. 1) is given by

$$q_L = \left(-K' \frac{\partial h'}{\partial z}\right)_{z=z_i'} \tag{7}$$

3. Green element formulations

The GE formulation of Eq. (5) that uses the transient Green's function in one spatial dimension has been presented in great detail in Taigbenu and Onyejekwe (1998) and summarized as well in Taigbenu and Onyejekwe (2000). It is worth noting that the model on which that formulation is based calculates the fluxes directly rather than by numerical differentiation of the hydraulic heads at the aquifer–aquitard interfaces, as commonly done in FE formulations. The two GE formulations for aquifer and aquitard flows proceed along the steps that have been presented in such references as Taigbenu (1995, 1999). These steps are summarized below:

(i) Obtain an appropriate auxiliary equation to the flow differential equation from which is derived the free-space Green's function;
(ii) Apply Green's second identity to both the auxiliary and flow differential equations to obtain the integral representation of the latter;
(iii) Discretize the flow region into suitable polygonal elements over which the distribution of the dependent variables is prescribed;
(iv) Within each element, derive a discretized form of the integral equation that is known as the element equation;
(v) Effect the boundary and initial conditions in the system of element equations;
(vi) Aggregate the element equations for all the polygonal elements, imposing the compatibility relations across element boundaries.

When the above steps are implemented, the resultant coefficient matrix is sparse and banded and, therefore, efficiently solved with commercially-available matrix solvers. For the case of the nonlinear unconfined aquifer flow, the element equations are linearized by the Picard algorithm in order that they can be solved.

3.1. Formulation for aquifer flow

To simplify the derivation of the GE formulation for the flow in the aquifers, the subscripts in Eqs. (1) and (2) are hereafter left out. Within a suitable polygonal element $\Omega^{(e)}$ that is used in discretizing the flow region, the medium is treated as homogeneous so that medium parameters for the entire flow domain assume piece-wise homogeneous variation. With that treatment, Eq. (1), for the confined aquifers, takes the following expression in each element

$$\bar{D}\nabla^2 h - \frac{\partial h}{\partial t} = -\bar{q}_L|_{z^t} + \bar{q}_L|_{z^b} + \bar{f}(x,y,t) + \bar{p} \tag{8a}$$

while for the unconfined case, Eq. (2) takes a similar expression

$$\bar{D}\nabla^2 h - \frac{\partial h}{\partial t} = \bar{q}_L|_{z^b} + \bar{f}(x,y,t) + \bar{p} \tag{8b}$$

in which $\bar{D} = \bar{T}/\bar{n}$, $\bar{q}_L = q_L/\bar{n}$, $\bar{f} = f/\bar{n}$ and $\bar{p} = p/\bar{n}$, where the bar on each of the quantities indicates their averaged values. Although Eqs. (8a) and (b) look quite similar, they are fundamentally different in the sense that Eq. (8a) is linear, whereas (8b) is not. We shall rewrite both equations as

$$\bar{D}\nabla^2 h - \frac{\partial h}{\partial t} = \bar{Q} + \bar{f}(x,y,t) + \bar{p} \tag{9}$$

where $\bar{Q}$ represents the net flux of water from overlying and underlying aquitards into the aquifer sandwiched between them. As earlier pointed out, this term is an input from the solution of the flow through the aquitards, which also depends on the hydraulic heads in the aquifers. It is evident how the solutions in the aquifers and aquitards are intertwined, thus necessitating the coupling of the models for both media.

The auxiliary equation to Eq. (9) is $\nabla^2 G - (\partial G/\partial t)/\bar{D} = \delta(r - r_i; t - \tau)$, and its solution in an infinitely extensive spatial domain is the Green's function that is given by:

$$G(r,t;r_i,\tau) = \frac{H(t-\tau)}{\bar{D}(t-\tau)} \exp\left[-\frac{(r-r_i)^2}{4\bar{D}(t-\tau)}\right] \tag{10}$$

Green's second identity is applied to both Eq. (9) and the auxiliary equation to give the integral

expression

$$\lambda h_i^{(2)} + \bar{D}\int_{t_1}^{t_2}\int_{\Gamma^{(e)}} [h(r,\tau)\nabla G(r,t_2;r_i,\tau)\cdot \mathrm{n} - G(r,t_2;r_i,\tau)\nabla h\cdot \mathrm{n}]\,\mathrm{d}\tau\,\mathrm{d}s - \int\int_{\Omega^{(e)}} G(r,\Delta t;r_i,0)h^{(1)}(r)\mathrm{d}A + \int_{t_1}^{t_2}\int\int_{\Omega^{(e)}} G(r,t_2;r_i,\tau) \times [\bar{Q}+\bar{f}+\bar{p}]\mathrm{d}A\,\mathrm{d}\tau = 0 \quad (11)$$

in which λ equals twice the nodal angle at the source node, and the superscripts 1 and 2, respectively, denote the previous time level t_1 and the current time level t_2. The above integral equation is similar to that expected from BE formulations, though it applies here to a typical element.

The numerical implementation of Eq. (11) is carried out with some distribution being prescribed for the functional quantities over the spatial element and in time. There is liberty in choosing that distribution, and as such we have in this work chosen a linear distribution in space and time so that a quantity, say h, has the general expression,

$$h = N_j(r)N^{(m)}(\tau)h_j^{(m)}; \quad j=1,2,\ldots g,\ m=1,2 \quad (12)$$

where g represents the number of nodes in the element, m is indicative of the time, with $m=1$ denoting the previous time and $m=2$ denoting the current time, and $N_j(r)$ and $N^{(m)}(\tau)$ are linear interpolation functions in space and time, respectively. It should be noted that the summation convention for a repeated index applies similarly to the superscripted index. The expression for the normal derivative of the Green's function is

$$\nabla G(r,t_2;r_i,\tau)\mathrm{n} = \frac{-\eta}{2\bar{D}(t_2-\tau)}G(r,t_2;r_i,\tau) \quad (13)$$

where η is the normal distance from the source node $r_i=(x_i,y_i)$ to the boundary over which integration is carried out (see Fig. 2). Introducing

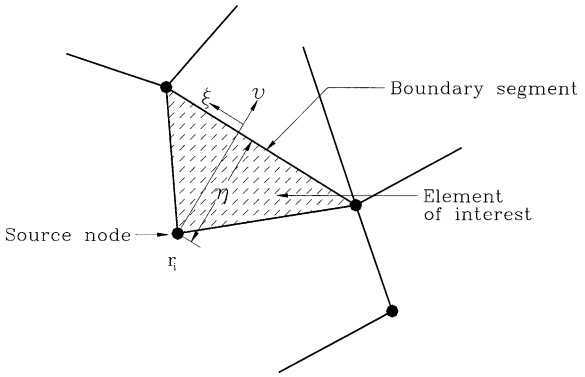

Fig. 2. Definition of normal distance from source node.

Eqs. (12) and (13) into Eq. (11) yields

$$\lambda h_i^{(2)} - \bar{D}\int_0^{\Delta t}\int_{\zeta_1}^{\zeta_2}\left[\frac{\eta}{2\bar{D}(\Delta t-\tau)}h_j^{(m)} + \frac{\partial h_j^{(m)}}{\partial n}\right] \times N_j(\zeta)N^{(m)}(\tau)G(\zeta,\Delta t;\zeta_i,\tau)\mathrm{d}\tau\,\mathrm{d}\zeta - \int\int_{\Omega^{(e)}} G(r,\Delta t;r_i,0)h_j^{(1)}\,\mathrm{d}A + \int_0^{\Delta t}\int\int_{\Omega^{(e)}} G(r,\Delta t;r_i,\tau) \times [\bar{Q}+\bar{f}+\bar{p}]\mathrm{d}A\,\mathrm{d}\tau = 0 \quad (14)$$

Eq. (14) can be expressed differently in terms of the normal boundary flux, $q=-\bar{T}\partial h/\partial n$ rather than, as presently the case, in terms of the normal derivative of the hydraulic head, $\partial h/\partial n$. In other earlier works, the incorporation of the normal boundary flux does not only enhance the accuracy of the numerical scheme, but also its convergence for nonlinear situations (Taigbenu, 2001a,b). The reason for this solution enhancement is because the formulation better preserves continuity of the flux at inter-element boundaries. It should be emphasized that the accurate evaluation of the boundary flux is critical in GE calculations as in BE computations; they have to be calculated directly as the hydraulic heads and should be done accurately to preserve the second order accuracy associated with the singular integral theory. Introducing the definition for the normal boundary flux into Eq. (14) yields, in matrix

form, the expression

$$B_{ij}^{(m)}h_j^{(m)} - S_{ij}h_j^{(1)} + L_{ij}^{(2)}q_j^{(2)} + L_{ij}^{(1)}\frac{\bar{T}^{(2)}}{\bar{T}^{(1)}}q_j^{(1)} + V_{ij}^{(m)}[Q_j^{(m)} + f_j^{(m)}] + P_i = 0 \quad (15)$$

in which

$$B_{ij}^{(m)} = \lambda\delta_{ij}\delta^{(m2)} - \frac{\eta}{2}\int_0^{\Delta t}\int_{\zeta_1}^{\zeta_2}\frac{1}{(\Delta t - \tau)} \times N_j(\zeta)N^{(m)}(\tau)G(\zeta,\Delta t;\zeta_i,\tau)\mathrm{d}\tau\mathrm{d}\zeta \quad (16a)$$

$$L_{ij}^{(m)} = \frac{1}{\bar{n}}\int_0^{\Delta t}\int_{\zeta_1}^{\zeta_2}N_j(\zeta)N^{(m)}(\tau)G(\zeta,\Delta t;\zeta_i,\tau)\mathrm{d}\tau\mathrm{d}\zeta \quad (16b)$$

$$S_{ij} = \int\int_{\Omega^{(e)}}G(r,\Delta t;r_i,0)N_j(r)\mathrm{d}A \quad (16c)$$

$$V_{ij}^{(m)} = \int_0^{\Delta t}\int\int_{\Omega^e}G(r,\Delta t;r_i,\tau)N_j(r)N^{(m)}(\tau)\mathrm{d}A\,\mathrm{d}\tau \quad (16d)$$

It should be pointed out that evaluation of the domain integrals does not present any additional computational challenges as in classical BE applications, and that is because the source and field nodes do always share the same element over which integration is carried out (Fig. 2). Special mention is made of the term that accounts for point sources and sinks, P_i. The ease with which it is evaluated in GE methodology makes the method most attractive for well hydraulics problems. Well contributions are only accounted for at nodes which belong to the elements in which wells are located, and for those elements the term P_i takes the form:

$$P_i = \frac{Q_w}{\bar{T}}E\left[\frac{(r_i - r_w)^2}{4\bar{D}\Delta t}\right] \quad (17)$$

where E is the Exponential integral. It is emphasized that Eq. (15) applies to a typical spatial element. The element equations depend largely on the geometric properties of the type of element used in discretizing the computational region. We are at liberty to choose the type of element, and in this work triangular and rectangular elements are incorporated into the numerical code.

An earlier paper discussed how the implementation of the integrations over the element can be done in such a manner that most of the integrals are evaluated exactly (Taigbenu, 2003a). Essentially it involves switching the order of carrying out the integrations in time and space. When an exact integration is not possible, the integration in the time dimension is first done to eliminate the singularity of the fundamental solution in time, and then integration in space is effected numerically. The boundary and domain integrals essentially yield three functions: Exponential Integral, Exponential and Error functions. Only the Exponential Integral exhibits a logarithmic singularity for small values of its argument, and decays more rapidly to zero than the Exponential function for relatively moderate values of argument, implying that the behaviour of the Exponential Integral is critical to the quality of the numerical solution. The expression for the argument, a dimensionless quantity, is

$$\psi = \frac{l^2}{4\bar{D}\Delta t} \quad (18)$$

where l is indicative of the element size. In cases where the spatial grid size has been determined, Δt is chosen so that ψ is not too large for its Exponential Integral to become too small, thereby producing a coefficient matrix that exhibits ill-conditioning characteristics. It is not expected that Δt be increased at infinitum; it has to have an upper limit which, for the advection-diffusion problem, is about a unit value of the Courant number (Taigbenu, 1999). The upper limit of Δt is largely dictated by the accuracy in approximating the primary variable in time by the interpolation function. This numerical feature of more stable and accurate solution with larger time step is computationally advantageous since it requires less number of simulation steps. Experiences gained from the current and previous works indicate that moderate values of ψ smaller than 4.0 give accurate results (Taigbenu, 2003b,c).

The global contribution of Eq. (15) for all the elements is achieved by aggregating the element equations in such a way that the nodal unknowns on the external boundaries are either h or q (whichever is not specified by the boundary conditions), and h at the internal nodes. This aggregation is done by keeping track of the compatibility requirements for the flux and hydraulic heads at inter-element

boundaries. In other words, the flux term is retained at all external boundaries, while boundary integrations on inter-element boundaries are not implemented with the source node on those boundaries because of the flux compatibility requirement that provides for the net contribution of the integrals to be zero. However, when the source node is not on an inter-element boundary, the boundary integrations of the flux term are implement with the flux expressed in terms of the head h. The contributions from all the elements constitute the global matrix equation:

$$A_{ij}u_j^{(2)} = R_i \tag{19}$$

where A_{ij} is a banded matrix and $u_j^{(2)} = \{h_j^{(2)}, q_j^{(2)}\}^T$ is a mixed vector of unknowns, and R_i is a known vector that accounts for the boundary, initial data, the leakage fluxes from the aquitards, and point and distributed recharge. For the unconfined aquifer flow case, the coefficient matrix A_{ij} is dependent on the water table elevation that has to be calculated in space and in time. The nonlinear discretized system of equations is linearized by the Picard algorithm by using known estimates of the hydraulic head in the coefficient matrix in carrying out the calculation of Eq. (19). The solutions obtained are compared with previous estimates until good agreement is achieved on the basis of a convergence criterion.

3.2. Formulation for aquitard flow

The GE formulation for the aquitard flow follows closely that earlier presented for the aquifers. An in-depth treatment of the formulation can be found in Taigbenu and Onyejekwe (1998). It uses the fundamental solution to $\partial^2 G/\partial z^2 + (\partial G/\partial \tau)/D' = \delta(z - z_i, t - \tau)$, that is

$$G(z,t;z_i,\tau) = \frac{H(t-\tau)}{[4\pi D'(t-\tau)]^{1/2}} \exp\left[-\frac{(z-z_i)^2}{4D'(t-\tau)}\right] \tag{20}$$

to construct the integral expression for Eq. (5). Green's identity is applied within a spatial element $[z_1, z_2]$ and integrated in time between t_1 and t_2 to obtain the integral equation

$$K'\left\{-\frac{h_i'(2)}{2} + \int_{t_1}^{t_2} [h'(z,\tau)G^*(z,t_2;z_i,\tau)]_{z=z_1}^{z=z_2}\,\mathrm{d}\tau\right\} + \int_{t_1}^{t_2} [q'(z,\tau)G(z,t_2;z_i,\tau)]_{z=z_1}^{z=z_2}\,\mathrm{d}\tau - C'\int_{z_1}^{z_2} h'(z,t_1)G(z,t_2;z_i,t_1)\mathrm{d}z = 0 \tag{21}$$

where $G^* = \partial G/\partial z$, $q' = -K'\partial h'/\partial z$, and $D' = K'/C'$. The variables h' and q' are approximated by linear interpolation functions in space and time, and the integrations in Eq. (21) are carried out to give

$$K'\left\{-\frac{h_i'(2)}{2} + \int_{t_1}^{t_2} [N^{(m)}(\tau)h'(m)G^*(z,t_2;z_i,\tau)]_{z=z_1}^{z=z_2}\,\mathrm{d}\tau\right\} + \int_{t_1}^{t_2} [N^{(m)}(\tau)q'(m)G(z,t_2;z_i,\tau)]_{z=z_1}^{z=z_2}\,\mathrm{d}\tau - C'\int_{z_1}^{z_2} N_j(z)h_j'(1)G(z,t_2;z_1;t_1)\mathrm{d}z = 0 \tag{22}$$

Eq. (22) is expressed in matrix form as

$$M_{ij}^{(m)}h_j'(m) + U_{ij}^{(m)}q_j'(m) = 0 \tag{23}$$

As in Eqs. (12) and (15), m is indicative of time. The analytical expressions of the matrices in Eq. (23) are found in Taigbenu and Onyejekwe (1998). Introducing the initial and boundary conditions (computed hydraulic heads in the overlying and underlying aquifers) into Eq. (23) gives a matrix equation that can be solved for $h'(2)$ and $q'(2)$. It is the values of $q'(2)$ at the aquifer–aquitard interfaces that are used for the leakage flux in the solution for the aquifers.

3.3. Coupling of aquifer and aquitard models

The coupling the aquifer flow model to that for the aquitards through the leakage fluxes at the aquifer–aquitard interfaces is fairly straight forward. At the start of each time step, the aquifer model is solved to obtain the hydraulic heads at the nodal points using known boundary and initial data and assuming the leakage flux is zero. The calculated heads in the aquifers become the boundary conditions for the aquitard model from which the leakage fluxes are calculated. These computed fluxes are then used as input into the aquifer model to obtained refined estimates of the hydraulic heads in the aquifers.

The process is repeated for a number of times till convergence for the entire aquifer–aquitard system is achieved. Convergence is considered attained when the mean deviation between current solution estimates and previous ones lies below a predetermined tolerance value.

4. Numerical examples

4.1. Example 1

The current numerical model for transient multi-aquifer flow is first demonstrated on an example that has an exact solution. It is that of radial flow into an infinitely extensive multiaquifer system comprising an aquitard sandwiched between two confined aquifers of which the lower one has a fully penetrating well discharging at a constant rate of 10.0 m^3/h. The exact solution is given by Neuman and Witherspoon (1969a) and represents the first exact solution to a truly multiaquifer system. The medium parameters of the two aquifers are the same: hydraulic conductivity $K = 3.3$ m/h, storativity $n = 10^{-5}$ and thickness of aquifer $b = 7$ m, while the parameters for the aquitard are: $K' = 3.696 \times 10^{-4}$ m/h, specific storage $C' = 10^{-5}$ m^{-1} and thickness of aquitard $b' = 16$ m. The flow problem has radial symmetry, and for that reason a $\pi/18$ sector of a circle with radius of 10^4 m is used as the computational domain. The domain is discretized into 31 triangular elements with a total of 33 nodes that are all on the boundary and arranged along the radial direction from the well at the positions $r = 1.0$, $10^{0.5}$, $10^{0.8}$, 10^1, $10^{1.25}$, $10^{1.5}$, $10^{1.8}$ 10^2, $10^{2.25}$, $10^{2.5}$, $10^{2.8}$, 10^3, $10^{3.25}$, $10^{3.5}$, $10^{3.8}$, 10^4 m. A no-flow condition is imposed on the boundaries along the radial direction, while zero drawdown is imposed at radius of10^4 m from the pumped well. In the numerical calculations, the location of the well, which is at the centre of the sector of the circle, is adjusted slightly by an amount of 10^{-5} m so that it is not at the same position as the node at the centre of the sector. It should be recognised that the position of the well is a singular point which should not be occupied by a node, thereby necessitating the adjustment. The convergence criterion used at each time step in simulating the coupled aquifer–aquitard flows is based on the mean absolute error (MAE) between consecutive iterates of the solution. With a value of 10^{-8} for the MAE, the computer program took no more than six iterations at each time step in achieving convergence. The numerical solutions are presented at radii of 10 and 100 m. The radial dimension is normalised to a dimensionless parameter that is expressed as $\beta_{11} = r/B_{11}$, where $B_{11} = 4b(KC/K'C')^{1/2}$. Those two radii where the numerical solutions are presented correspond to $\beta_{11} = 0.01$ and $\beta_{11} = 0.1$. Fig. 3a and b show the numerical and analytic solution of Neuman and Witherspoon (1969a) which are in terms of the variation of the dimensionless drawdown $h_D = 4\pi Th/Q_W$ with respect to the dimensionless time $t_D = Kt/(Sr^2)$. The results of GEM, referred to as model 1, are based on the logarithmic Green's function formulation of Taigbenu and Onyejekwe (2000), while those referred to as model 2 are based on the current GE formulation. We observe that the GE solutions are in good agreement with the analytical solution. The solutions of the two GE models do exhibit the same trend, despite being obtained from two different Green's functions. The wiggles in the numerical solution of the hydraulic head in the pumped aquifer are probably as a result of the very small distance between the pumped well and the first node at the centre which is not accurately evaluated in the argument of the Exponential Integral.

4.2. Example 2

This second example is a reduced form of example 1. It is presented here in order to evaluate the performance of the current formulation in handling groundwater well hydraulics in single aquifers. This example addresses both the cases of flow to a single well in an infinitely confined aquifer that has an exact solution that is given by Theis (1935) and flow to a leaky confined aquifer overlain by a uniform-head watertable aquifer whose solution is given by Hantush and Jacob (1955). For the latter case storage effects are neglected in the leaky stratum, thereby providing for a linear variation in the hydraulic head across the aquitard. The same computational domain and discretization as in example 1 are used in this example with prescribed conditions being incorporated into the numerical code. The numerical results from the current formulation, those of model 1 and analytic

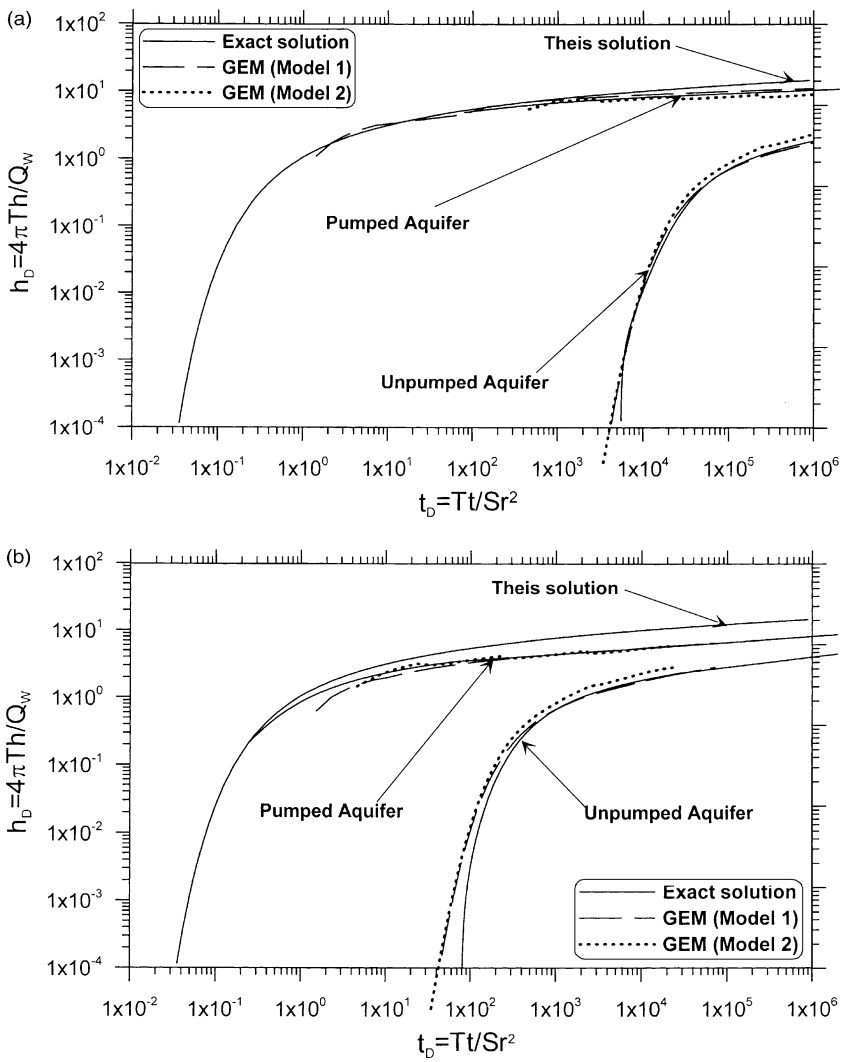

Fig. 3. GEM and exact solutions of drawdown for two-aquifer example at (a) $\beta_{11} = r/B_{11} = 0.01$, (b) $\beta_{11} = r/B_{11} = 0.1$.

solutions at r/λ of 0.01 and 0.1 $\left(\lambda = \sqrt{bb'K/K'}\right)$ are presented in Fig. 4. It can be observed that there is good agreement between the GE model solutions and the exact.

4.3. Example 3

This third example is one that represents a physically realistic flow in a multiaquifer system that consists of four aquifers that are separated by three aquitards. The areal extent of the aquifer is about 12 km^2 and it is shown in all subsequent figures of this paper. The hydrogeological parameters of the aquifers and aquitards are given in Table 1a. Two flow scenarios are examined: the first is one in which the uppermost aquifer (aquifer 4) is confined, and the second in which the uppermost aquifer is unconfined. In all the four aquifers, 17 active wells are in operation and their abstraction rates and locations are given in Table 1b. It is only for simplicity that we have designed the problem so that the thicknesses of the aquifers and aquitards are uniform; as stated earlier, this is not intended to suit the GE models that are herein applied.

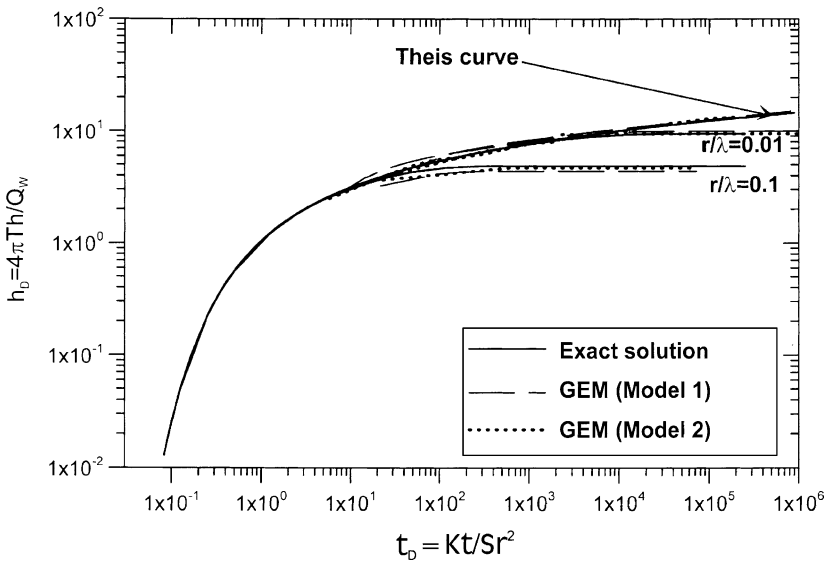

Fig. 4. Comparison of GEM and exact solutions for example 2.

For both flow scenarios, the piezometric head in all confined aquifers (water table elevation for the unconfined aquifer) at the initial time is 180 m. That head is maintained on segments CD and EF at all times, while on segment AB the hydraulic head is raised to 190 m for times later than the initial time. On segment DE, a uniform normal flux of 0.36 m^3/d per metre length of boundary is allowed into the aquifer for all times, while the segments BC, FG, and GA act

Table 1a
Hydraulic parameters for example 3

Medium	Hydraulic conductivity [m/d]	Thickness [m]	Storage coefficient [m^{-1}] (confined) or specific yield (unconfined)
Aquitard 1	3.1×10^{-3}	11.5	1.1×10^{-5}
Aquitard 2	1.1×10^{-3}	18.2	4.8×10^{-5}
Aquitard 3	6.4×10^{-4}	9.4	2.2×10^{-5}
Aquifer 1 (confined)	8.4	30.0	2.6×10^{-4}
Aquifer 2 (confined)	2.2	43.0	7.2×10^{-5}
Aquifer 3 (confined)	1.5	37.0	5.0×10^{-4}
First flow scenario			
Aquifer 4 (confined)	5.4	14.0	6.2×10^{-4}
Second flow scenario			
Aquifer 4 (unconfined)	5.4		0.2

Table 1b
Abstraction rates and location of wells for example 3

Location		Strength m^3/d
x_w[m]	y_w[m]	
Wells in aquifer 1		
3715.4	1478.0	
4314.3	2421.3	1180.0
412.7	1845.5	1360.0
3528.1	1476.0	1201.0
1645.2	2483.6	1170.0
Wells in aquifer 2		
3173.88	1105.0	
3833.8	2342.43	1125.0
1750.7	1870.16	1270.0
2776.2	958.51	1470.0
Wells in aquifer 3		
1972.29	1440.0	
902.2	1999.02	1180.0
1820.7	1113.42	1250.0
2480.1	2805.11	1570.0
Wells in aquifer 4		
3374.0	1011.0	
4296.5	1512.4	1360.0
1180.4	1428.7	1406.0
2519.8	1432.8	1390.0

as no-flux boundaries. With these conditions incorporated into the two GE models, a uniform time step of 2 days is used in the current model and 1day in model 1. The flow region, being irregular, is discretized with triangular elements which closely matched the irregular boundaries. In all, the region is discretized with 3624 triangular elements with lengths of the sides of the elements ranging from 50 to 200 m. These elements constitute a total of 1848 nodes. The nodes are optimally numbered to achieve a half band width of 88 for the global coefficient matrix. The vertical line segments that are used in representing the flow in the aquitards are discretized with 7 nodes on each of them. The nodes are generated by Chebyshev polynomials so that they are closer to each other near the aquifer–aquitard interfaces than the middle of the aquitard. This is helpful in capturing the high hydraulic gradients when the interface is stressed at small times. In each of the aquifer, the equipotential lines at times of 10 and 20 days are plotted. These plots are presented in Figs. 5–8. Using a global MAE between consecutive solution iterates of 10^{-4}, no more than 5 iterations were required to achieve convergence at each simulation interval in both models. In general, less number of iterations was required as the solution times increased, indicating that the numerical scheme is stable. This trend lends support to earlier findings when the GEM was applied to nonlinear flow problems (Taigbenu, 2001a,b). Running the computer codes of models 1 (with logarithmic Green's function) and model 2 (current model) on a Pentium III PC, the first model took 5 min 31.09 s, whereas the current model took 4 min 5.84 s for the entire 20 days simulation of this example. Noting that model 1 used 20 simulation steps, while model 2 used ten, the former model runs at about 48% faster per simulation step than the current one.

For the first flow scenario, there is generally good agreement between the solutions from the two GE models. In aquifer 1, the cone of depression of well located close to the upper boundary AB is submerged by the influx from the recharge boundary along AB. The influx of water through DE has virtually no influence on the wells closest to that boundary (Fig. 5a and b). In aquifer 2 where all wells are located at some distance from the recharge boundaries of AB and DE, their cones of depression are distinctly preserved (Fig. 6a and b). The flows into the wells essentially dictate the general flow pattern in this aquifer. The flow pattern in aquifer 3 follows that observed earlier in aquifer 2 with the cones of depression around the wells being distinct (Fig. 7a and b). The cones of depression around the wells, though expanding with time, remain quite distinct and unaffected by the influx of water from the recharge boundaries AB and DE. For the uppermost confined aquifer 4, the cones of depression of the four wells stand out quite distinctly at times of 10 and 20 days, with relatively flat piezometric head distribution outside the wells at the former time (Fig. 8a and b). However, at time of 20 days, while there now exist enlarged cones of depression at all the wells; the piezometric head distribution outside the wells is no longer as flat, with a gradient southward. It is also significant to note that the well on the southwest boundary DE has, because of its strength, greater influence on the flow than the influx of water into the aquifer through that boundary.

In the second flow scenario of this example, the topmost aquifer is now an unconfined one and receives natural recharge at a constant rate of 100 mm/year uniformly over the entire aquifer. The bottom of the unconfined aquifer is taken to be at an elevation of 125 m, so that the saturated thickness of the unconfined aquifer at the initial time is 55 m. While model 1 incorporated a uniform time step of 1 day in its simulation, the current model was run with an increased time step of 2 days. Because of the large difference between the specific yield of the unconfined aquifer and the storativity for the confined aquifer, ψ in Eq. (18) is larger for the unconfined aquifer than the confined one. With increased time step, ψ is reduced and consequently manageable values of the Exponential integral are obtained (Taigbenu, 2003b,c). The results of the simulations from the two models are presented only at time of 20 days in Figs. 9–12. There is again good agreement between the solutions of models 1 and 2. As expected there is little difference between the piezometric heads in aquifers 1, 2 and 3 for the current flow scenario and the previous one. That is observed by comparing Figs. 5b and 9 for aquifer 1, Figs. 6b and 10 for aquifer 2, and Figs. 7b and 11 for aquifer 3. However, when it comes to the topmost aquifer, there are substantial differences between water table distribution of the unconfined aquifer 4 and the confined aquifer 4 of the previous flow scenario. The differences are not only

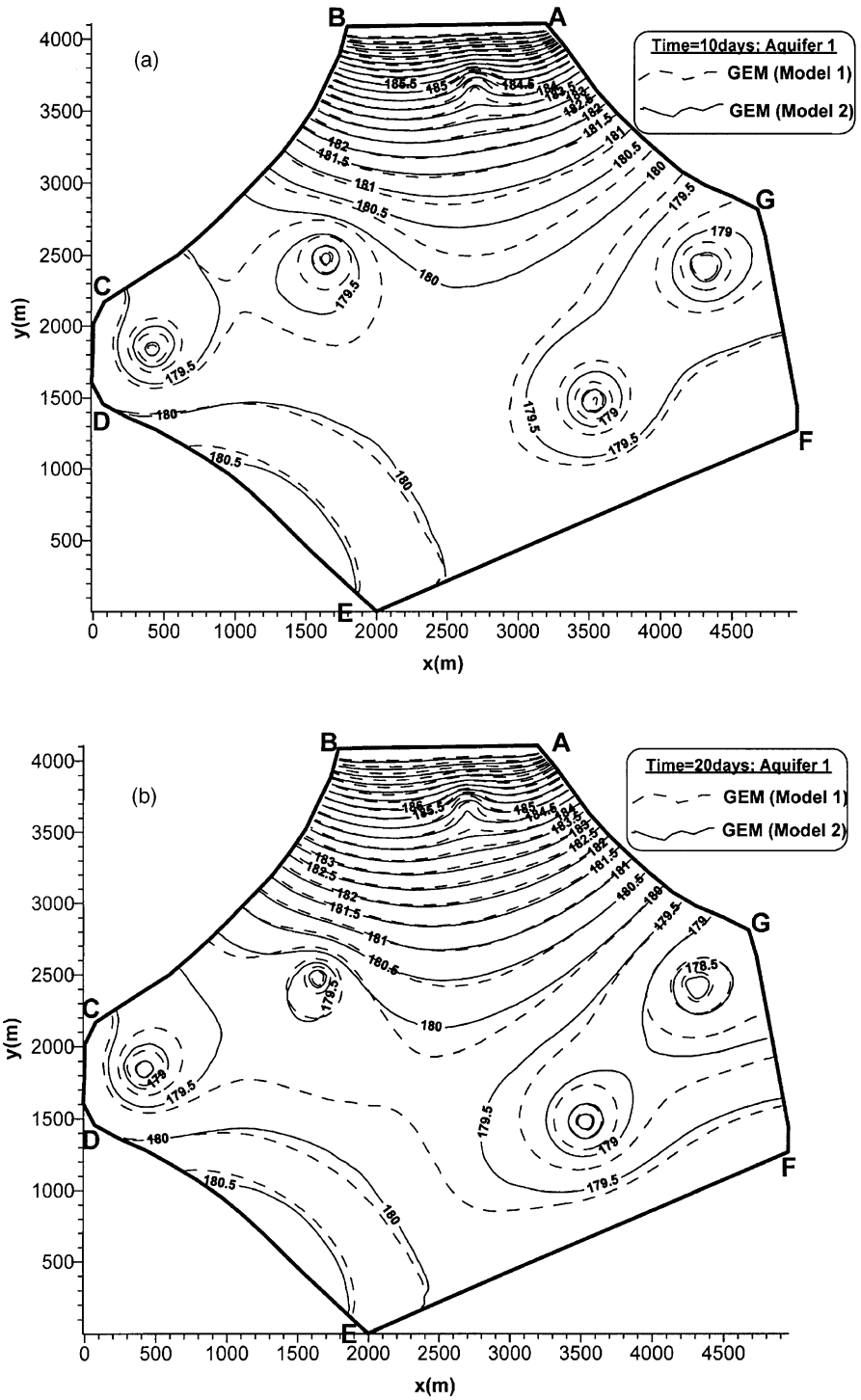

Fig. 5. Contour of piezometric head in confined aquifer 1 of first flow scenario of example 3 at (a) time = 10 days, (b) time = 20 days.

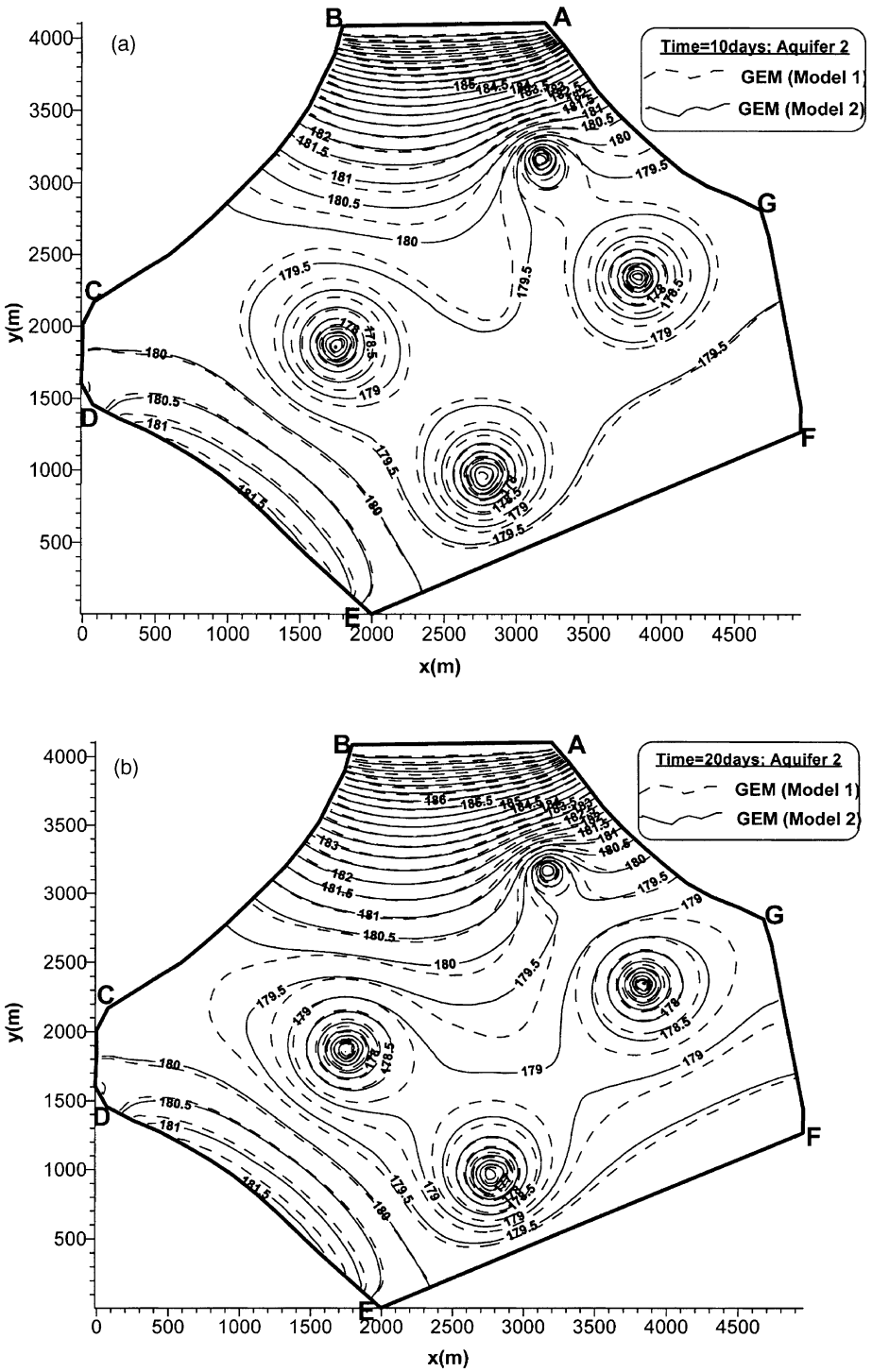

Fig. 6. Contour of piezometric head in confined aquifer 2 of first flow scenario of example 3 at (a) time = 10 days, (b) time = 20 days.

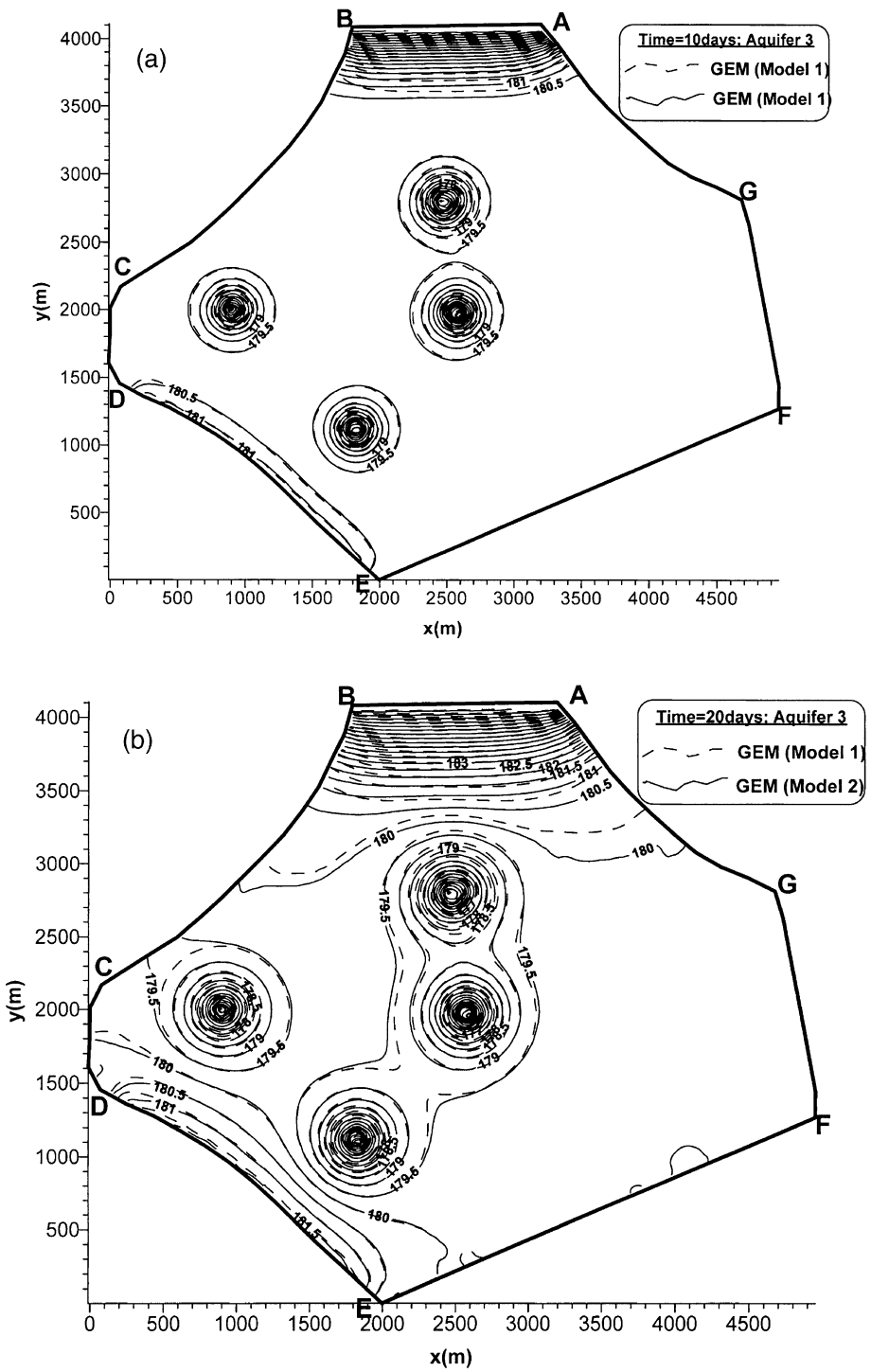

Fig. 7. Contour of piezometric head in confined aquifer 3 of first flow scenario of example 3 at (a) time = 10 days, (b) time = 20 days.

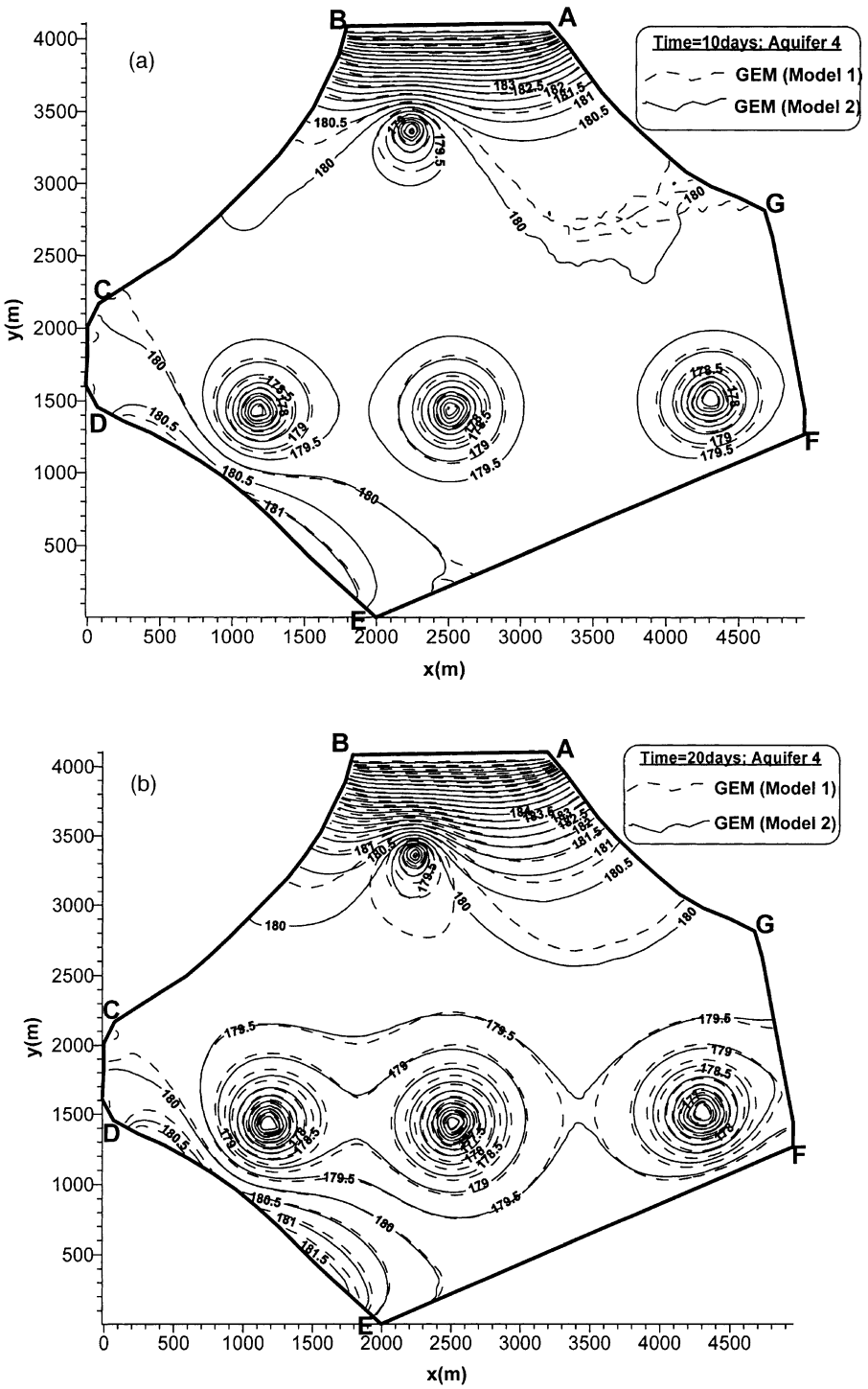

Fig. 8. Contour of piezometric head in confined aquifer 4 of first flow scenario of example 3 at (a) time = 10 days, (b) time = 20 days.

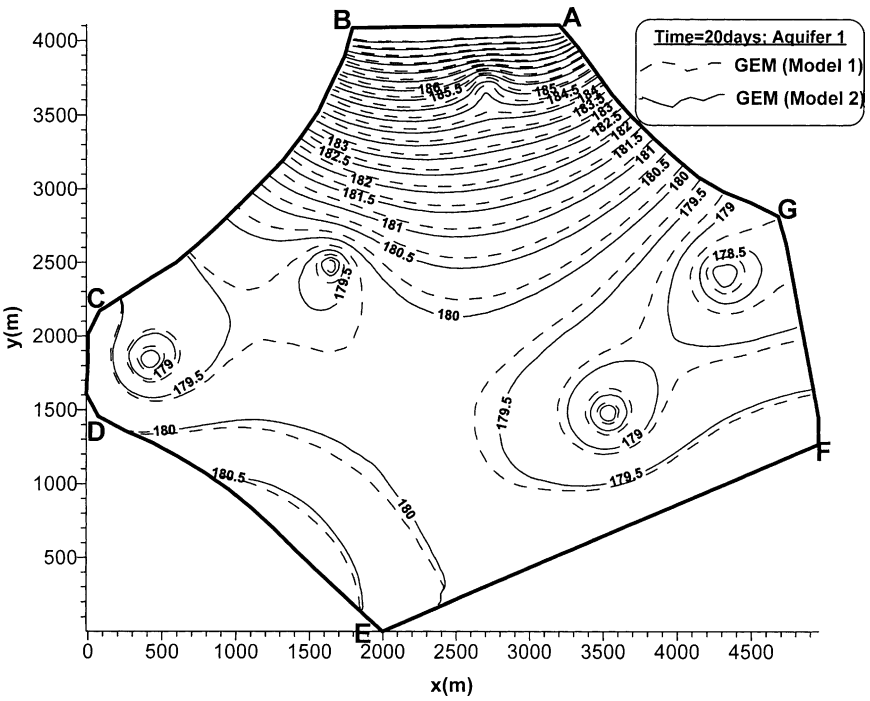

Fig. 9. Contour of piezometric head in confined aquifer 1 of second flow scenario of example 3 at time = 20 days.

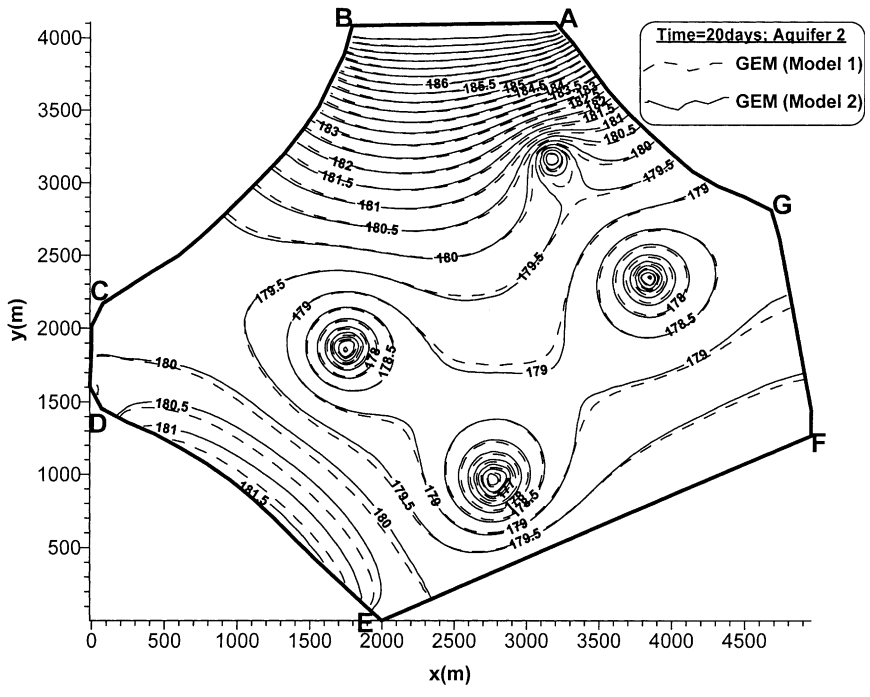

Fig. 10. Contour of piezometric head in confined aquifer 2 of second flow scenario of example 3 at time = 20 days.

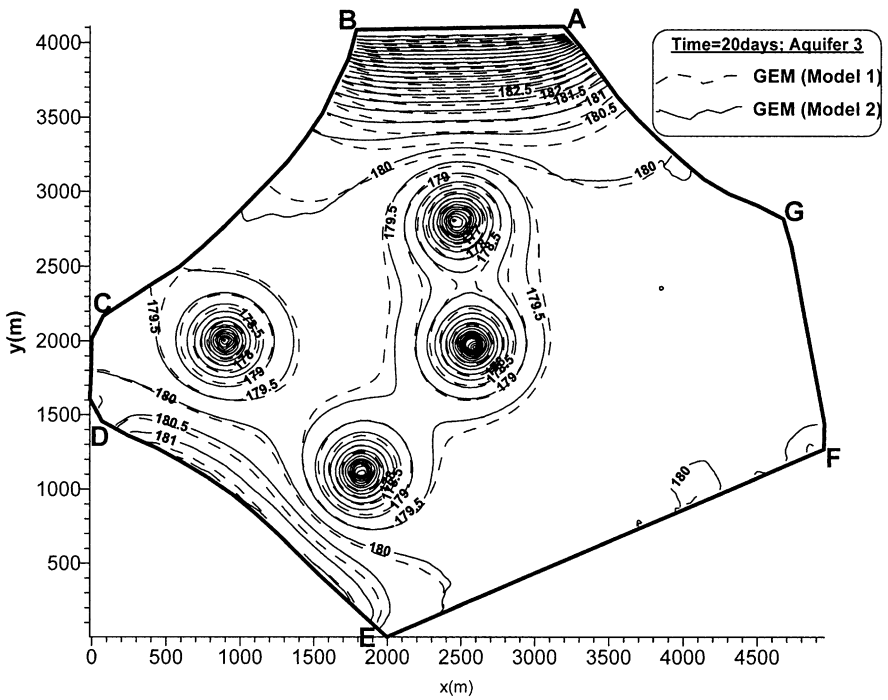

Fig. 11. Contour of piezometric head in confined aquifer 3 of second flow scenario of example 3 at time = 20 days.

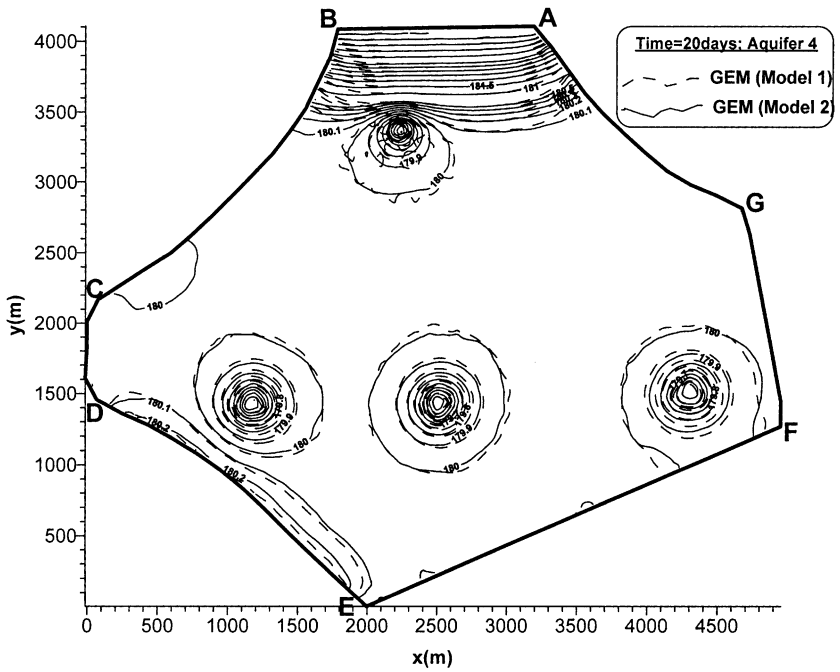

Fig. 12. Contour of water table in unconfined aquifer 4 of second flow scenario of example 3 at time = 20 days.

due to the fact that we are dealing with different types of aquifers but also because of the recharge being admitted in the unconfined aquifer. The water table is relatively flat at an elevation of about 180 m while the cone of depression at the wells is much more limited than into the confined case because of the small elastic property associated with unconfined aquifers. It should be noted that contour increments had to be reduced to 0.1 m to be able to obtain any meaningful contour of water table elevations in the unconfined aquifer (Fig. 12). In addition, the area of influence of the recharge through the flux boundary DE is a lot more curtailed in the current flow scenario.

5. Conclusion

This paper has presented another viable solution strategy on the basis of the GEM for transient flows in multi-aquifer systems of arbitrary geometries with any number of alternating layers of aquifers and aquitards, and pumping and recharge stresses. It retains the accurate leakage flux-predicting formulation of an earlier model (Taigbenu and Onyejekwe, 2000), but uses the 2-D Green's function of that formulation for the evaluation of the flow and storage of water in the aquifers. One obvious advantage of the current model is that there is consistency in the Green's function employed for the flows in the aquitards and aquifers. However, the current model runs slower than the previous one because of the more complicated functions that have to be evaluated.

On existing examples of two confined aquifers sandwiched by an aquitard (Witherspoon, 1969a), of flow into a confined aquifer overlain with an unconfined aquifer maintained at uniform water table elevation (Hantush and Jacob, 1955), and flow to a confined aquifer (Theis, 1935), all of which have exact solutions, the current model has accurately reproduced those solutions. The capabilities of the current model are explored with a realistic multi-aquifer flow example, and its solutions are comparable to those from the earlier model of Taigbenu and Onyejekwe (2000). The current model, thus, provides an alternative solution approach to solving transient multiaquifer flows.

Acknowledgements

In carrying this work, the financial support from the Swedish International Development Cooperation Agency (SIDA) under the water-related research project at the National University of Science and Technology (NUST) is acknowledged. Furthermore, the author is grateful to two reviewers whose comments were very useful in revising the original manuscript.

References

Bear, J., 1979. Hydraulics of Groundwater, McGraw-Hill Book Company, NY.

Cheng, A.H-D., Morohunfola, O.K., 1993. Multilayered leaky aquifer systems: 2. Boundary element solutions. Water Resour. Res. 29, 2801–2811.

Cheng, A.H-D., Ou, K., 1989. An efficient Laplace transform solution for multiaquifer systems. Water Resour. Res. 25, 742–748.

Chorley, D.W., Frind, E.O., 1978. An iterative quasi-three-dimensional finite element model for heterogeneous multi-aquifer systems. Water Resour. Res. 14, 943–952.

Hantush, M.S., Jacob, C.E., 1955. Nonsteady radial flow in an infinite leaky aquifer. Eos Trans. AGU 36, 95–100.

Herrera, I., 1970. Theory of multiple leaky aquifers. Water Resour. Res. 6, 185–193.

Herrera, I., Yates, R., 1977. Integrodifferential equations for systems of leaky aquifers and applications: 3, A numerical method of unlimited applicability. Water Resour. Res. 13, 725–732.

Jacob, C.E., 1946. Radial flow in a leaky artesian aquifer. Eos Trans. AGU 27, 198–208.

Neuman, S.P., Witherspoon, P.A., 1969a. Theory of flow in a confined two-aquifer system. Water Resour. Res. 5, 803–816.

Neuman, S.P., Witherspoon, P.A., 1969b. Applicability of current theories of flow in leaky aquifers. Water Resour. Res. 5, 817–829.

Premchitt, J., 1981. A technique in using integrodifferential equations for model simulation of multiaquifer systems. Water Resour. Res. 17, 162–168.

Strack, O.D.L., 1999. Principles of the analytic element method. J. Hydrol. 226, 128–138.

Taigbenu, A.E., 1995. The Green element method. Int. J. Numer. Methods Engng. 38, 2241–2263.

Taigbenu, A.E., 1999. The Green Element Method, Kluwer Academic Publishers, Boston.

Taigbenu, A.E., 2001. Unsaturated-Flow Simulation with Green Element Models. ASCE J. Hydraul. Engng. 127, 307–312.

Taigbenu, A.E., 2001. Simulations of unsaturated flow in multiply zoned media by Green element models. Transport Porous Media 45, 387–406.

Taigbenu, A.E., 2003a. Features of a time-dependent fundamental solution in the Green Element Method. Appl. Math. Model. 27 (2), 125–143.

Taigbenu, A.E., 2003b. Green element calculations of nonlinear heat conduction with a time-dependent fundamental solution. Engineering Analysis with Boundary Elements (in press).

Taigbenu, A.E., 2003c. A time-dependent Green's function-based model for stream-unconfined aquifer flows. Water SA 29 (3), 257–265.

Taigbenu, A.E., Onyejekwe, O.O., 1998. Green's function-based integral approaches to linear transient boundary-value problems and their stability characteristics (I). Appl. Math. Model. 22, 687–702.

Taigbenu, A.E., Onyejekwe, O.O., 2000. A flux-correct Green element model of quasi three-dimensional multiaquifer flow. Water Resour. Res. 36 (12), 3631–3640.

Theis, C.V., 1935. The relationship between the lowering of the piezometric surface and the rate and duration of discharge of a well using ground-water storage. Eos Trans. AGU 16, 519–524.

Zakikhani, M., Aral, M.M., 1989. Direct and boundary-only solutions of multilayer aquifer systems. Part B. Unsteady-state solution. J. Hydrol. 111, 69–87.